IMPROVED PERFORMANCE OF ULTRA-HIGH MOLECULAR WEIGHT POLYETHYLENE FOR ORTHOPEDIC APPLICATIONS

A Thesis

by

KEVIN PLUMLEE

Submitted to the Office of Graduate Studies of
Texas A&M University
in partial fulfillment of the requirements for the degree of

MASTER OF SCIENCE

December 2008

Major Subject: Mechanical Engineering

IMPROVED PERFORMANCE OF ULTRA-HIGH MOLECULAR WEIGHT POLYETHYLENE FOR ORTHOPEDIC APPLICATIONS

A Thesis

by

KEVIN PLUMLEE

Submitted to the Office of Graduate Studies of
Texas A&M University
in partial fulfillment of the requirements for the degree of

MASTER OF SCIENCE

Approved by:

Chair of Committee,	Christian Schwartz
Committee Members,	Hong Liang
	Melissa Grunlan
Head of Department,	Dennis O'Neal

December 2008

Major Subject: Mechanical Engineering

ABSTRACT

Improved Performance of Ultra-High Molecular Weight Polyethylene for Orthopedic Applications. (December 2008)

Kevin Plumlee, B.S. Mech. Eng., Oklahoma Christian University

Chair of Advisory Committee: Dr. C. J. Schwartz

A considerable number of total-joint replacement devices used in orthopedic medicine involve articulation between a metallic alloy and ultra-high molecular weight polyethylene (UHMWPE). Though this polymer has excellent wear resistance, the wear particulate produced leads to the limited lifetime of the devices – osteolytic bone loss. Crosslinking has been shown to reduce the wear rate of UHMWPE, but can cause a reduction in various mechanical properties such as impact toughness. This study presents two alternate approaches to improving the wear performance of UHMWPE in orthopedic applications

Previous work has shown that UHMWPE-based composites have wear resistance comparable to the irradiation-crosslinked polymer. Zirconium has been shown to have excellent corrosion resistance and biocompatibility, and the authors have used the material as reinforcing filler in UHMWPE with promising results. Compression-molded UHMWPE composites with up to 20 weight percent (wt%) of micro-sized zirconium particles were investigated with regards to wear behavior and impact toughness. These

composites showed a significant reduction in wear compared to unfilled polymer while still maintaining impact toughness. These results reinforce the paradigm of using polymer composites for orthopedic applications and may provide a viable alternative to the property tradeoffs encountered with irradiation crosslinking.

Apart from UHMWPE, novel materials including hydrogels and bio-derived polymers show great potential in orthopedics, but such materials require the development of innovative fixation techniques [1-3]. The development of controlled porous UHMWPE morphologies offers the opportunity to utilize and expand these developing technologies. Interconnected porous structures were prepared by dry mechanical mixing of NaCl particles and UHMWPE powders followed by compression molding. Samples were soaked in water to remove the embedded salt, leaving a porous UHMWPE structure. Computational simulations of porogen distribution and leaching predicted leaching to be 95% effective when initial salt concentrations were 60wt% and higher, which was found to match very well with the experimental data. It was found that varying the concentration and particle size of the porogen can tailor the final pore morphology to a specific application, while DMA results showed that storage and loss moduli depend greatly on porosity, but not on pore size. Finally, porous UHMWPE scaffolds were successfully impregnated with gelatin, confirming the compatibility of UHMWPE with hydrogel-based fillers.

.

ACKNOWLEDGEMENTS

I would like to thank my committee chair, Dr. Schwartz, and my committee members, Dr. M. Grunlan and Dr. H. Liang, for their guidance and support throughout the course of this research. Their constant willingness to offer support, and the encouraging manner in which it was given, was the most important lesson I hope to take home.

I would also like to thank the Texas A&M microscopy center, especially Ann Ellis and Mike Pendleton, for their assistance with the procedures, materials, and equipment, and for giving so much of their time in an effort get high quality electron microscope images. Also, a special thank you is extended to Dr. J Grunlan and Dr. H.J. Sue for access to their facilities and equipment.

Thanks also go to my friends and colleagues for allowing me to pick their brains, steal their ideas, and generally slow everything down. The relationships I have developed during my research have made Texas A&M University a second home as well as a pleasant learning environment. Finally, my parents deserve all the thanks I can muster.

NOMENCLATURE

UHMWPE	Ultra-high molecular weight polyethylene
Zr	Zirconium
NaCl	Sodium Chloride
wt%	Percent of sample, by weight
vol%	Percent of sample, by volume
μm	Micrometers
nm	Nanometers
J	Joules
m	Meters
SEM	Scanning Electron Microscope
DAWS	Dual Axis Wear Simulator
DMA	Dynamic Mechanical Analysis
QC	Quasicrystals

TABLE OF CONTENTS

Page

ABSTRACT iii

ACKNOWLEDGEMENTS v

NOMENCLATURE vi

TABLE OF CONTENTS vii

LIST OF FIGURES viii

LIST OF TABLES x

1. INTRODUCTION 1

2. IMPROVED WEAR RESISTANCE OF ORTHOPEDIC UHMWPE BY REINFORCEMENT WITH ZIRCONIUM PARTICLES 3

    2.1 Introduction 3
    2.2 Materials and Methods 6
    2.3 Results and Discussion 11
    2.4 Conclusions 22

3. ORTHOPEDIC POTENTIAL FOR POLYMER-PROTEOGLYCAN COMPOSITES THROUGH DEVELOPMENT OF POROUS UHMWPE MORPHOLOGIES 23

    3.1 Introduction 23
    3.2 Materials and Methods 26
    3.3 Results and Discussion 30
    3.4 Conclusions 46

4. GENERAL CONCLUSIONS 48

REFERENCES 49

VITA 57

LIST OF FIGURES

Page

Figure 1 The Dual Axis Wear Simulator with a close up of sample holders and counterface shaft 7

Figure 2 Schematic of Dual Axis Wear Simulator behavior 8

Figure 3 SEM images of zirconium particle distribution in unfilled UHMWPE, 10 wt% zirconium sample, and 20 wt% composite 12

Figure 4 Visual representations of counterface surface roughness when unworn (a), worn by unfilled UHMWPE (b), worn by 10 wt% Zr (c), and worn by 20 wt% Zr (d)..... 144

Figure 5 SEM images taken of wear surfaces from unfilled UHMWPE (a, b), 10 wt% Zr (c, d), and 20 wt% Zr (e, f)..... 17

Figure 6 Fracture surface of unfilled UHMWPE and 20 wt% Zr composite.. 20

Figure 7 SEM images of fracture surface from impact toughness tests..... 21

Figure 8 Representations of sample cross-sections from a numerical model which simulates the distribution of porogen and matrix particles during dry powder mixing..... 31

Figure 9 Numerical model predictions of final porosity for a 6x6x15mm sample filled with porogen particles of varying size..... 34

Figure 10 Final Porosity results: theoretical predictions and experimental data 36

Figure 11 SEM images of porous UHMWPE structures created through salt leaching 38

Page

Figure 12 DMA measurements of storage and loss modulus for porous samples made with varying contents of small NaCl particles. 39

Figure 13 Comparison of storage and loss modulus for samples made from large and small NaCl particles. 40

Figure 14 Secondary image and backscattered image of a 30% porous sample made from large NaCl particles. 41

Figure 15 Comparison of gelatin penetration for samples made with (a) 30% porous, large particles; (b) 30% porous, small particles; (c) 50% porous, large particles; (d) 50% porous, small particles. 42

Figure 16 Backscattered images of voids in a porous sample made using large NaCl particles. 44

Figure 17 Gelatin can flow through the narrow channel at (c), which measures 20 μm across. However, gelatin does not flow through channel (d), which measures only 10 μm across. 45

LIST OF TABLES

Page

Table 1 Surface roughness of wear counterface after wear tests.....13

Table 2 Wear results after 250k cycles. 15

Table 3 Impact toughness results for zirconium composites. 19

1. INTRODUCTION

Modern artificial joints are comprised of an articulating metal component that slides against a polymer bearing surface. Ultra-high molecular weight polyethylene (UHMWPE) has remained the material of choice for use as the bearing component since applications since its debut in orthopedic applications in the 1950's. UHMWPE has excellent properties in terms of durability, coefficient of friction, and wear rate; however, its long term performance *in vivo* is limited. Over an extended period of use, a small amount of wear debris is liberated from the bulk UHMWPE. As this microscopic wear particulate accumulates around the implant, it triggers a complex immune system response, the result of which is a state of net bone loss surrounding the implant. This condition, known as osteolysis, causes joint pain, loosening, and ultimately limits the lifespan of an artificial joint.

To combat the osteolytic effect and extend the life expectancy of artificial joints, many researchers have crosslinked the UHMWPE. This technique drastically reduces the wear of UHMWPE, thereby reducing the osteolytic effect. Unfortunately, crosslinking has a negative effect on other material properties, namely impact toughness. This thesis considers different approaches to improving the wear performance of UHMWPE in artificial joints. The first approach, , follows the recent paradigm in research of developing UHMWPE composites which have the potential for increasing the wear resistance and impact performance through the use of appropriate fillers. The

---

This thesis follows the style of *Wear*.

study described in Section 2 of this work presents results of a UHMWPE-based composite filled with zirconium particles.

The second approach explored in this work is based on an entirely different approach to reducing the osteolytic effect, and is described in more detail in Section 3. As opposed to decreasing the volume of wear particulate that forms over time, this technique aims at making the wear debris less harmful to the body. Novel bio-derived polymers and hydrogels have shown a high degree of biocompatibility and biodegradation, but lack the structural durability required for orthopedic applications. This study explores the viability of merging the benefits of both UHMWPE and hydrogels through the creation of tailored porous UHMWPE scaffolds, then impregnating the scaffold with a gel-based material.

2. IMPROVED WEAR RESISTANCE OF ORTHOPEDIC UHMWPE BY REINFORCEMENT WITH ZIRCONIUM PARTICLES

2.1 Introduction

Total Hip Arthroplasty (THA) is a commonplace procedure, though for younger patients there is a need to develop new materials that can extend the life of the artificial joint beyond 20 years. Modern devices have a bearing surface of ultra-high molecular weight polyethylene (UHMWPE) which has a low coefficient of friction and a low wear rate. However over time, wear particulate does accumulate leading to a condition known as osteolysis, which leads to bone loss, joint loosening, discomfort, and ultimately limits the lifespan of the joint.

Crosslinking, either through irradiation or chemical reactions, dramatically reduces the wear rate of UHMWPE, effectively prolonging the onset of osteolysis. Unfortunately, studies have often shown that some mechanical properties (impact toughness in particular) are compromised [6-11]. Current research efforts are being directed towards reducing the wear rate of UHMWPE without sacrificing the impact toughness typically associated with crosslinking. While this front is being pursued through many different approaches, a great deal of research has focused on using acetabular cups made entirely from ceramic materials. Zirconia (zirconium oxide) has recently proven to be a viable material for use in ceramic joints, having extremely low wear while exhibiting biocompatibility [12, 13]. Early studies show that osteolysis plays a lessened role in zirconia joints; however, ceramic joints are not without their

downfalls, including lower fracture toughness than metal-on-polymer hips, reported noise, and poor wear performance when paired with other zirconia components [13].

Another possible technique for reducing wear is the use of composites, which has shown promise due to the ability to dramatically improve a variety of mechanical and thermal properties of polymers through the use of selected fillers. Much of this research has looked into using fillers in UHMWPE specifically for improving its performance in artificial joints. This includes the addition of naturally found biomaterials for increased biocompatibility [14, 15], and the inclusion of polydimethylsiloxane for increased ductility [16]. The recent interest in nanotechnology has led to the addition of many different nanoparticles such as carbon nanotubes [17-19], and nanoclay platelets, both for increased strength and stiffness [20]. However, it is not clear whether these fillers are biocompatible in the manner in which they have been proposed to be used. Many filler materials, especially nano-sized fillers, require strong interfacial bonding between filler and matrix in order to reach maximum effectiveness. However, hard, rigid fillers not only share in the compressive load distribution of the polymer matrix without the need of strong interfacial bonding, but they also modify the crystallization process by creating nucleation sites. Xiong *et al.* noticed this phenomenon using aluminum oxide nanoparticles [21]. The weak points in the crystalline structure can also serve as cavitation sites for deformation, generating greater plastic deformation than in pure samples. Tanniru *et al*. also observed an increase of UHMWPE impact toughness when filled with calcium carbonate nanoparticles [22].

Previous research into a UHMWPE composite filled with platinum-zirconium quasicrystals (QC) showed that such an approach provided excellent mechanical properties while reducing wear by amounts comparable to crosslinking [23]. While this filler material showed excellent biocompatibility, the platinum component and the quasicrystal fabrications methods lead to prohibitive material costs. However, the behavior of the QC filler was surmised to be due to its inherent mechanical properties more so than chemistry, and thus it may be reasonable to identify another biocompatible mechanical filler material that is less costly but will provide comparable wear benefits. This study took a preliminary look at improving the wear and mechanical properties of UHMWPE by creating a composite filled with zirconium microparticles. It was hypothesized that as the acetabular cup wears, the zirconium particles exposed to the surface will deform and possibly work-harden, thus shielding the surrounding polymer regions from the shear stresses that produce wear during joint motion.

To investigate a material's potential benefit for use in THA devices, accelerated wear tests are often performed that simulate the conditions found *in vivo*. Various wear parameters have been shown to be relevant in simulated testing, including wear path geometry, lubricant composition, load, and surface roughness of the components [12, 24, 25]. In this study, the authors have preliminarily explored the use of embedded zirconium microparticles as method to enhance the performance of UHMWPE in THA applications. In particular, wear tests were performed with both unfilled UHMWPE and zirconium composites so that wear rates and mechanisms could be compared. Also, the

impact toughness of the materials was studied as an identifier of possible mechanical property impairment that often results from crosslinking.

2.2 Materials and Methods

Wear Testing

The Dual Axis Wear Simulator (DAWS), shown in Figure 1, was developed as a screening device for examining the effectiveness of various materials as bearing surfaces in THA applications. A detailed description and validation of the test apparatus have been reported previously [26]. To do this, nine samples were individually affixed to dedicated pneumatic cylinders via nylon collets. Six of these nine sample holders are held in a carriage which translates laterally via a motor-driven lead screw, while the remaining three sample holders remain stationary and serve as soak control samples. When the pneumatic cylinders held in the carriage are engaged, the samples are extended to contact a 25.4 mm diameter shaft which lies below the carriage. As the carriage translates, the samples slide along the length of the shaft. This shaft also rotates perpendicularly to the motion of the carriage, giving the DAWS setup two degrees of freedom (Fig. 2). Both the carriage and counterface shaft are driven by computer-controlled motors, providing the capability to coordinate complex wear path geometries. While the DAWS machine features interchangeable counterfaces, this study employed a cobalt-chrome alloy shaft (BioDur® CCM®, Carpenter Technology Corporation), polished to a surface roughness of 0.2 μm R_a as the wear counterface.

The three remaining sample holders remain stationary, applying load to a separate and stationary shaft similar to the wear counterface shaft. These three samples experience loading and environmental conditions equivalent to the wear samples, but do not wear, thereby serving as soak control samples to compensate for fluid absorption. All of the samples and wear interfaces are contained in a heated basin which can be filled with protein enriched solutions to more accurately reproduce *in vivo* conditions.

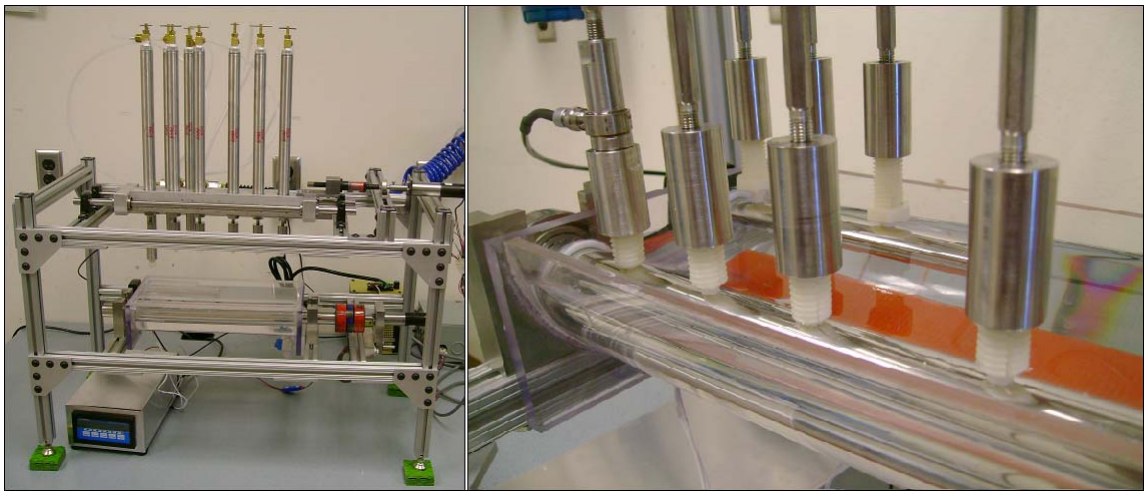

Figure 1: The Dual Axis Wear Simulator (left) with a close up of sample holders and counterface shaft (right).

Materials

Granulated ultra-high molecular weight polyethylene, (GUR-1050, Ticona) was used to produce unfilled UHMWPE samples as well the composites. Zirconium particles, 3 μm in diameter (Sigma-Aldrich) were received as a suspension in a 1:10

solution of pentanol in water. The particles were dried and weighed in a nitrogen environment to prevent oxidation. Once thoroughly dried, the particles were added to UHMWPE powder to create 10 and 20 percent zirconium mixtures, by weight, which were then mechanically mixed using a vortex mixer until each powder mixture reached a uniform gray color.

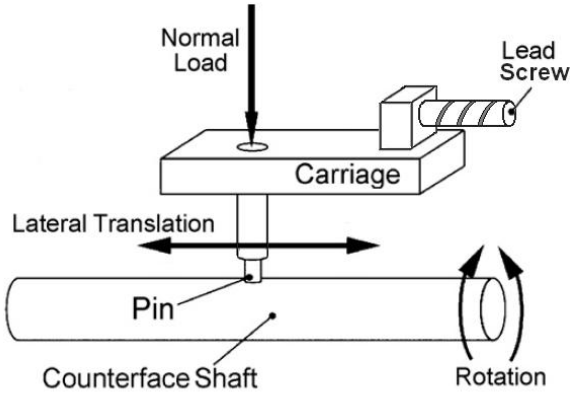

Figure 2: Schematic of Dual Axis Wear Simulator behavior. Adapted from [26]

Wear Testing Procedure

Wear pins were produced by compression molding in a heated press. The powder mixtures were compressed in cylindrical mold at 100 MPa for 10 min at a platen temperature of 230°C to obtain samples 6.3 mm in diameter and approximately 17mm long. The wear surface of each pin was smoothed using progressively finer sand paper

(400-1200 grit). Three different fill contents were tested: pure UHMWPE, 10 and 20 weight percent Zr, with a total of six sample pins created for each. Four of the six pins were used as wear samples, while the remaining two samples were used as soak control samples. The test order and position within the machine were randomized.

Wear tests were performed in lubricant consisting of 25% bovine calf serum (HyClone) diluted with distilled and de-ionized water. To reduce dissolution and microbial growth, the lubricant contained 20 mM of pH balanced EDTA and 1% penicillin-streptomycin-neomycin solution (Sigma Aldrich). The lubricant was heated to a target temperature of 37° C for the duration of the presoak and wear test. All samples were soaked in the lubricant for 24 hours prior to wear tests. Samples were then washed in an ultrasonic bath, first for 15 min in soapy water, then for 15 min in distilled water. Lastly, the samples were soaked in methanol for 5 min, then left to dry for 15 min. The mass of each sample was then recorded.

All pins were subjected to a load of 70 N for the duration of the test. This produced a calculated Hertzian contact pressure of approximately 3.0 MPa. The soak control samples remained stationary, while the wear pins were subjected to 250,000 cycles, with the wear path of each cycle consisting of a 6.4 x 6.4 mm square. Each cycle lasted 0.65 seconds, resulting in a relative speed of 38 mm/sec. After the completion of the test, all samples were washed according to the process described above, then re-weighed. The mass loss of each wear sample was then corrected for fluid absorption using the corresponding weight loss of the soak control samples. This value was then converted into volume lost using the density of the samples.

Impact Toughness Testing

Impact samples were created using the same powder mixtures described previously. The powder mixtures were compression molded in a 63x12.5x8 mm mold at 230° C and 4 MPa for 10 min. The samples were left to cool in ambient room temperature conditions, and then notched in the center of their length on both sides according to the appropriate ASTM standard [27]. Izod impact tests were performed on a TMI Impact Tester, model 43-02, which recorded the energy of breaking. The cross sectional area of the un-notched portion of the sample was recorded after breaking and the impact toughness was calculated.

Imaging

Images of both wear samples and impact samples were taken in a JOEL-6400 scanning electron microscope (SEM), and were prepared using a ruthenium vapor coating method [28], then lightly sputter-coated with gold-palladium. Sections of impact samples were cut with razor blades, and then imaged in both secondary mode and backscatter mode. The high atomic number of zirconium resulted in bright spots in backscattered images, revealing the distribution of particles within the samples.

The surface roughness of the counterface shaft was measured with a Zygo NewView 600s non-contact profilometer. After the completion of the wear tests, the counterface showed visible damage at the wear interfaces, so roughness measurements

were taken on unworn portions of the shaft, as well as on the wear interfaces for selected samples.

2.3 Results and Discussion

Particle Distribution

Scanning electron images from both the secondary and backscattered modes were compared to reveal distribution of zirconium particles within the matrix, as seen in Figure 3. The images revealed that the particles accumulated in long veins that ran through the entirety of the samples. This can be explained by the difference in particle size between the zirconium and the UHMWPE during the mixing state, causing the smaller zirconium particles (3 μm) to gather in the empty regions between larger UHMWPE particles (100-300 μm). Other than the groupings caused by the particle geometries, the zirconium particles did not appear to naturally agglomerate together even when in close proximity, suggesting that dispersion could be improved by simply altering the initial particle size of the UHMWPE powder, with a diameter ratio of 1:1 resulting in the most uniform distribution.

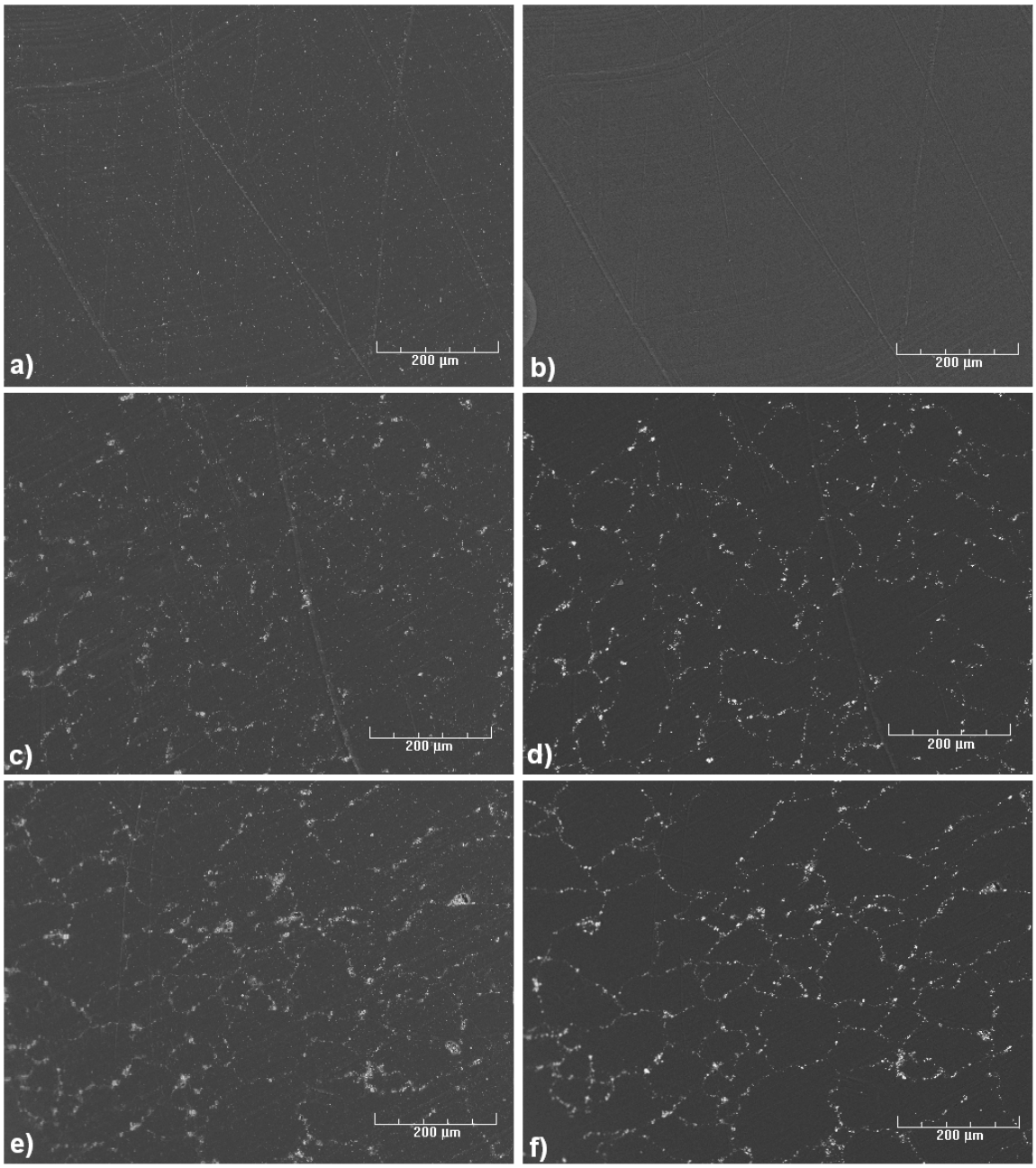

Figure 3: SEM images of zirconium particle distribution in unfilled UHMWPE (a, b), 10 wt% zirconium composite (c, d), and 20 wt% composite (e, f). Secondary images (a, c, e) show surface features while back-scattered images (b, d, f) show heavy zirconium particles.

Individual zirconium particles appear to be fully encompassed by UHMWPE, confirming that the melted polyethylene was able to flow around the zirconium particles during the molding process. However, in the regions between polyethylene powder particles, many zirconium particles accumulated. The extremely small crevices between these closely packed particles, along with the high melt viscosity of UHMWPE, led to voids where the melted polymer could not penetrate. Since this was not observed with individual particles, it is assumed that better dispersion would lead to increased mechanical properties.

Visual inspection of the wear counterface upon the completion of the wear tests revealed that the shaft appeared more polished within the wear traces of the zirconium-filled samples than within the traces of the unfilled samples. This was further verified by surface roughness measurements, which are listed in Table 1 and seen in Figure 4. This data suggests that the presence of zirconium is a relevant factor in counterface wear; however, further study is necessary to determine the extent of this relationship.

Table 1: Surface Roughness of wear counterface after wear tests

Sample Type	Counterface Roughness, R_a (μm)
Initial Roughness	0.169
UHMWPE	0.184
10 wt% Zr	0.068
20 wt% Zr	0.092

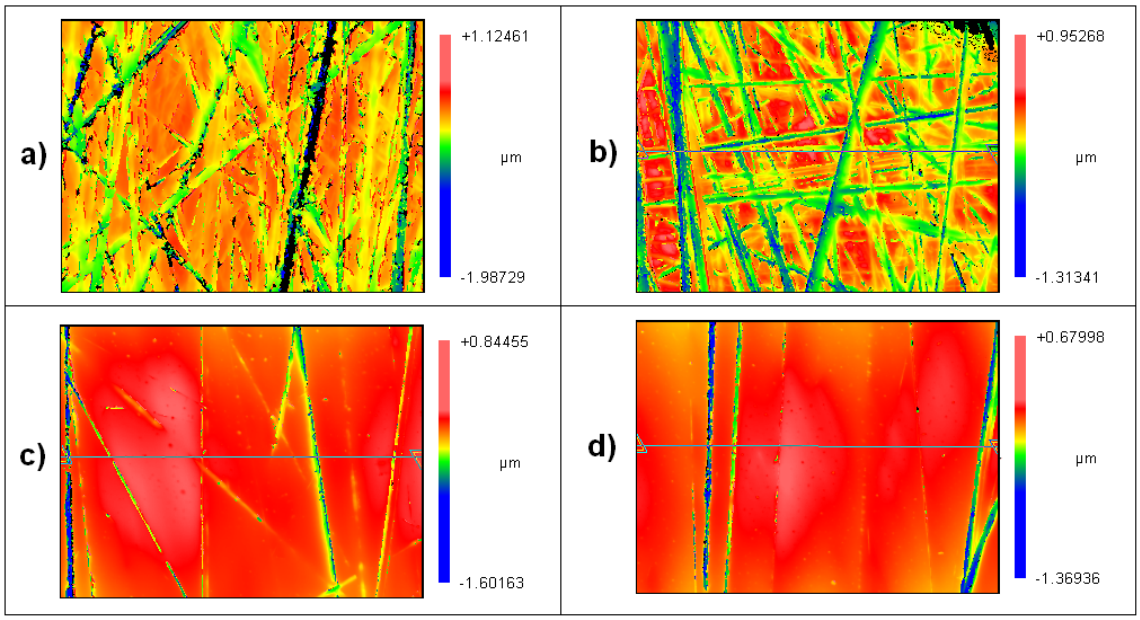

Figure 4: Visual representations of counterface surface roughness when unworn (a), worn by unfilled UHMWPE (b), worn by 10 wt% Zr (c), and worn by 20 wt% Zr (d).

Wear Test Results

Masses of the samples were recorded before and after wear tests. This data was compensated for moisture absorption and converted to volume lost. The sample standard deviations and mean weight loss was calculated for each fill content. These results are shown in Table 2. This information was then analyzed for statistical significance using a two-tailed T-test, revealing a difference between the unfilled UHMWPE and 10 wt% wear ($p = 0.19$), and between UHMWPE and 20wt% wear ($p = 0.06$). There may have also been a slight difference between mean wear of the 10 wt% and 20 wt% samples, although the significance was much lower ($p = 0.39$).

Table 2: Wear Results after 250k cycles. Values calculated from four wear samples and two soak control samples.

Sample Type	Wear Volume (mm^3)	
	Mean	Standard Deviation
UHMWPE	0.4945	0.0985
10 wt% Zr	0.3685	0.0831
20 wt% Zr	0.3109	0.0385

SEM images of the resultant wear surfaces were taken from two samples of each of the fill contents tested, as seen in Figure 5. At high magnification, all of the samples revealed the same characteristic ridged surface associated with UHMWPE wear, suggesting that same wear mechanisms were present for each sample at a microscopic level. The ridged surface is typically attributed to motion and alignment of crystalline lamella and the plastic deformation of the neighboring amorphous region. Typically, crosslinking reduces the distance between these folds due to decreased polymer chain mobility. However, the samples from this study revealed ridges that were equally spaced for both unfilled and filled samples, suggesting that the material properties of the UHMWPE at this scale were unaltered by the presence of zirconium particles. It was also observed that the exposed zirconium particles were flattened but had little surface features, as seen in the upper left corner of Figure 5(c). This implies that the zirconium particles underwent plastic deformation as opposed to wear. In doing so, the particles likely support a large portion of the load that would normally fall upon the polymer

matrix, thereby stress-shielding the local polymer. This is in agreement with the stress-shielding model proposed in previous work [23].

These characteristic wear patterns also suggest that the main method for material removal was high strain of surface asperities due to shear and cyclic loading. The majority of the material removal occurred while the samples were translated laterally, that is, in parallel with the counterface shaft axis. This effect was seen in previous tests on the DAWS testing apparatus, and can be explained by two major factors: 1) the counterface shaft was originally polished on a lathe so that the majority of the polishing grooves run radially around the shaft, making the shaft rougher in the axial direction than in the radial direction; and 2) the rotation of the counterface shaft (radial motion) helps to bring fresh lubricant into the wear interface, while lateral motion does not. This leads to more aggressive wear and sticking in the lateral direction.

At lower magnifications, the zirconium-filled samples showed signs of delamination, including fissures, material folding and separations, which can be seen in Figure 5. The unfilled UHMWPE did show some level of deformation in surface profile, although the surface had fewer separations and remained relatively continuous. It is suspected that this discrepancy is due to the poor dispersion of particles within the composites, which creates a path of weak regions within the polymer matrix. When the polymer is cyclically loaded, fatigue cracks can quickly propagate around the boundaries of the zirconium particles, creating separated regions which can deform more freely and independently of each other.

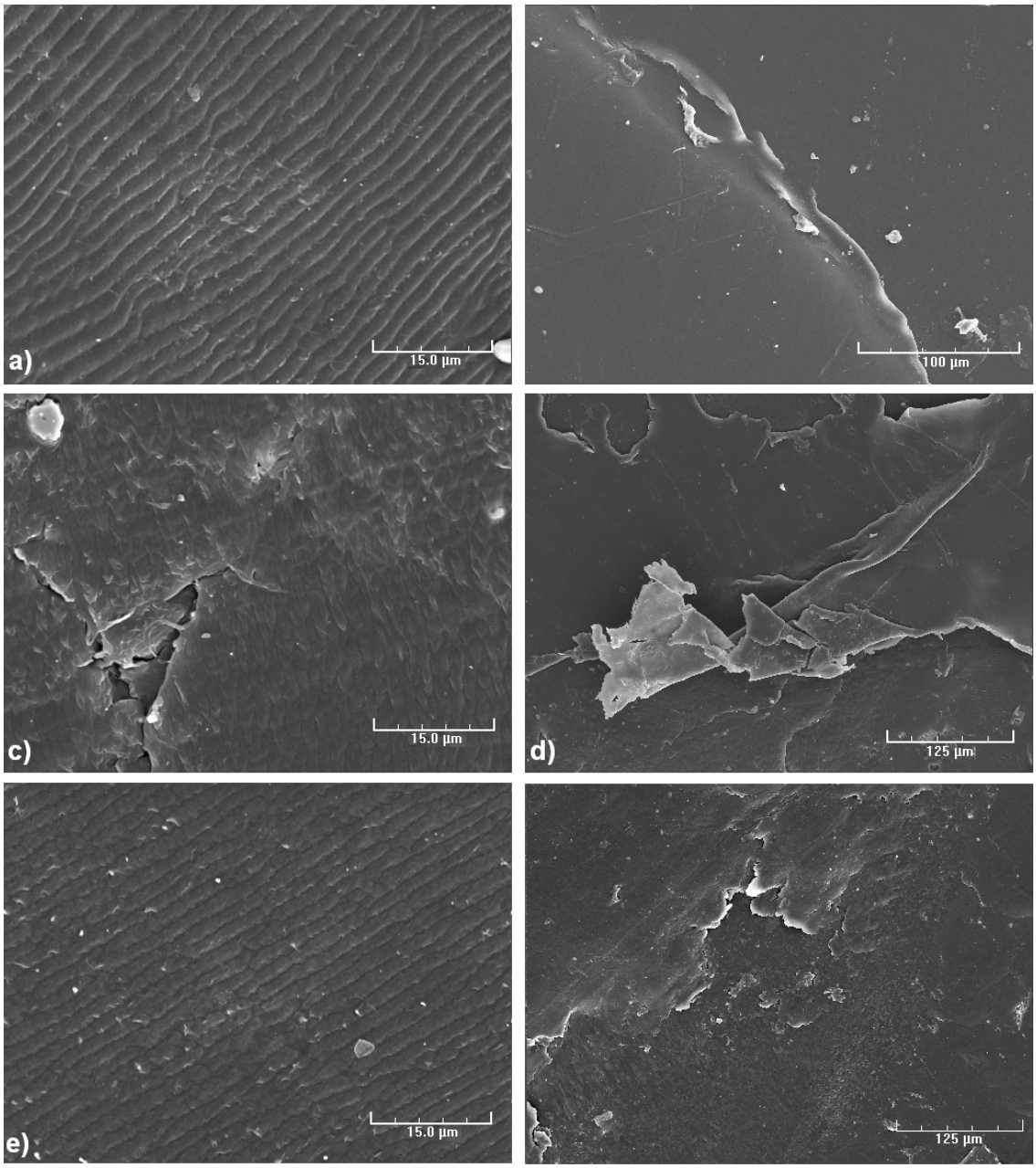

Figure 5: SEM images taken of wear surfaces from unfilled UHMWPE (a, b), 10 wt% Zr (c, d), and 20 wt% Zr (e, f). A zirconium particle can be seen in the upper left corner of (c).

It is likely that a more uniform distribution of particles would further slow the wear rate of the composite by providing uniform stress shielding conditions, and making crack propagation more difficult. It also may be possible to increase the bond strength between the zirconium and polyethylene through the use of chemical treatments in an effort to decrease crack propagation, but doing so may hinder the wear performance of the composite. Firstly, a stronger bond between particle and matrix would require that when the particle begins to plastically deform under load, more of that load is transferred to the matrix, decreasing the stress-shielding effectiveness. Secondly, as cracks spread, larger regions may flake off as wear particulate, which would likely not initiate an osteolytic response if the particles exceed a critical size. Lastly, the spreading of cracks through the boundary areas may help reduce the transmission of shear stresses throughout the bulk sample.

Impact Results

Impact toughness results, shown in Table 3, show no significant difference between unfilled UHMWPE and 10 wt% zirconium samples, with a p-value of 0.985, reflecting that the means were the equal. This is in contrast to crosslinking, which trades off a decrease in impact toughness with an increase in wear resistance. The 10 wt% samples reduced the wear rate of UHMWPE while maintaining impact toughness.

Table 3: Impact toughness results for zirconium composites. Values calculated from four samples.

Sample Type	Izod Impact Toughness (J/mm^2)	
	Mean	Standard Deviation
UHMWPE	0.105	0.011
10wt% Zr	0.105	0.019
20wt% Zr	0.082	0.011

The 20 wt% samples were significantly less tough than pure samples ($p = 0.116$), showing a decrease of approximately 20% in impact toughness. However, the SEM images reveal that in the cases of the 20 wt% composites in particular, cracks were able to propagate through weak points within the large particle agglomerations (Fig. 6). Similar findings were observed in the 10 wt% samples, although to a lesser extent. This suggests that improved dispersion would lead to improved impact toughness for both 10 wt% and 20 wt% composites. For the case of 10 wt%, this could lead to impact toughness higher than the original unfilled UHMWPE. Other SEM images reveal relatively smooth fracture surfaces on unfilled UHMWPE, while zirconium filled samples have markedly rougher surfaces (Fig. 7). Since a rougher surface often suggests an increase in impact toughness, this further confirms the idea that improved dispersion could lead to an increase in impact toughness, especially in higher fill contents. This is particularly important since the wear results indicate that higher fill contents produce lower wear rates.

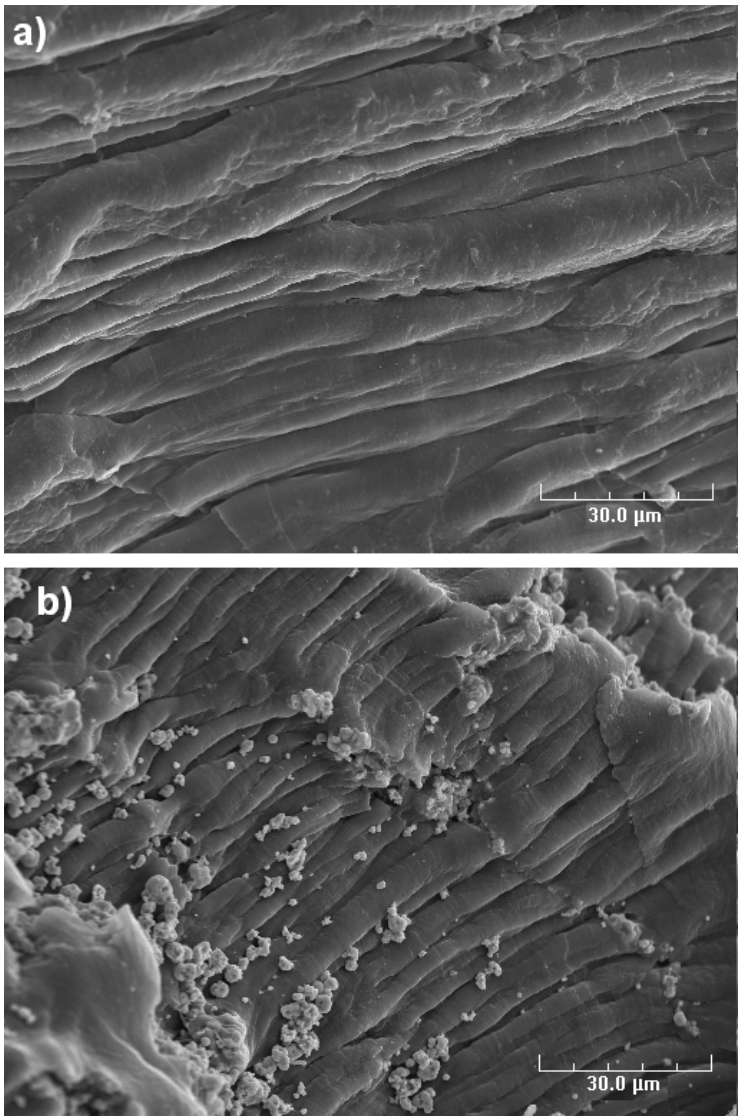

Figure 6: Fracture surface of (a) unfilled UHMWPE and (b) 20 wt% Zr composite. Notice the excess of zirconium particles along the fracture surface of the composite, suggesting that the crack propagated around their boundaries.

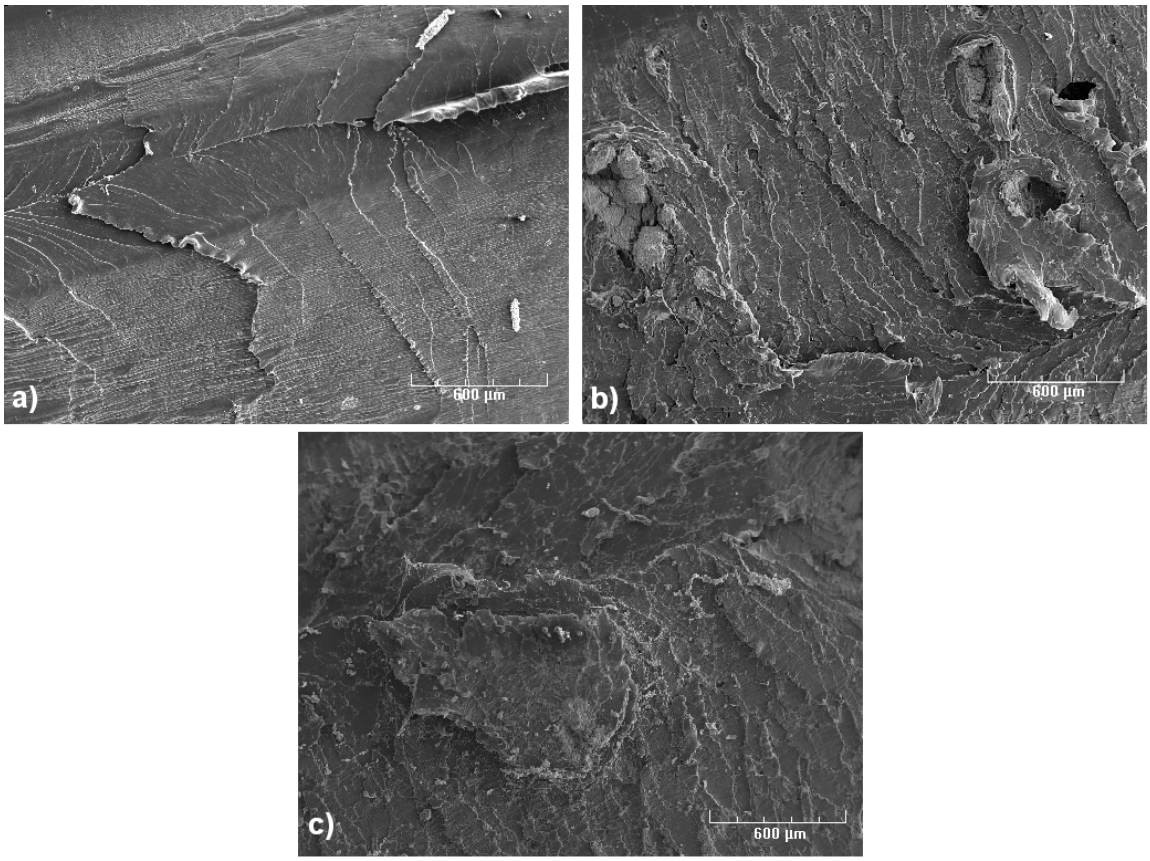

Figure 7: SEM images of fracture surface from impact toughness tests. Unfilled UHMWPE (a), 10wt% Zr (b), 20wt% (c)

Recent studies of nanocomposites suggest that using smaller filler particles may create more dramatic results using lower filler amounts. This could potentially improve both impact toughness and wear reduction. However using such small particles may require alternate mixing techniques to maintain adequate dispersion. Further study is necessary to determine the specific mechanisms and properties which the zirconium particles influence within the polymer matrix. Factors of interest include the level of oxidation of the zirconium particles once in a finished sample form, the viscoelastic

behavior of the composite, and the crystallization mechanisms of the composite. Also, material properties of the composite should be measured, such as hardness, toughness, stiffness, and ultimate strength.

2.4 Conclusions

1. Zirconium microparticles can effectively be dispersed into UHMWPE using a dry powder mixing process. For the most uniform dispersion, the UHMWPE particle size should be equal to the zirconium particle size.
2. The inclusion of zirconium particles into a UHMWPE matrix can effectively reduce the wear rate of the component without sacrificing the impact toughness.
3. While the reduction in wear particulate generated is anticipated to slow the rate of osteolysis, the inclusion of zirconium particles may increase the wear of a metal counterface, which requires future investigation as to *in vivo* performance.

3. ORTHOPEDIC POTENTIAL FOR POLYMER-PROTEOGLYCAN COMPOSITES THROUGH DEVELOPMENT OF POROUS UHMWPE MORPHOLOGIES

3.1 Introduction

Ultra high molecular weight polyethylene (UHMWPE) remains the most popular material for bearing surfaces in artificial joint applications. Despite its high durability, low coefficient of friction, and biocompatibility in bulk form, studies have revealed that wear particulate shed from UHMWPE is responsible for initiating osteolysis, a degeneration of the bone surrounding the implant, which ultimately limits the lifespan of the device[4].

A great deal of research has centered on slowing down this process by decreasing the production rate of wear particulate. Crosslinking has been shown to significantly reduce the wear rate of UHMWPE [9, 29-31], but also decreases elongation at break and impact toughness [7, 10, 32, 33]. To overcome this deficiency associated with crosslinking, many researchers have turned to composites. Tanniru *et al* found the inclusion of inorganic calcium carbonate particles increased the impact toughness of UHMWPE by up to 50 percent to counteract the detriment caused by crosslinking [22]. Guofang *et al* incorporated the mineral kaolin during UHMWPE polymerization and reduced the wear rate by over 40% such that crosslinking may no longer be necessary [34]. Similar results were found using quartz [35], alumina [21], quasicrystals [23], carbon fiber [36], and a variety of nano-fillers such as carbon nanotubes [19]. The use

of more compliant materials, both as a stand-alone bearing material [26] and as a composite constituent [16, 37], can reduce contact pressures and friction coefficients at wear interfaces, thereby reducing the total wear rate.

As opposed to simply decreasing the wear volume, another possible solution revolves around making the wear debris exhibit less potential for osteolysis. Many researchers have explored this avenue by filling UHMWPE with materials naturally found in the human body, including hyaluronan [14] and hydroxyapatite [38]. In general, these types of fillers duplicate the wear reduction seen with inorganic composite fillers, but still fail to create structures and behavior that mimic natural cartilage found in healthy joints. Studies have shown that osteolysis is triggered predominately by wear particles between 0.1-1 μm in diameter [39, 40], with the most of the wear particulate falling within this range [41, 42]. Therefore, modifying the material such that the wear debris is drastically larger or smaller may reduce the osteolytic effect.

Current trends in biomedical research revolve around materials that more closely approximate living tissue. In particular, hydrogels have found numerous applications as scaffolds, drug delivery media, and as cell growth stimulants [43]. A hydrogel's capacity in mimicking the extracellular matrix of living soft tissues makes them prime candidates for use as synthetic cartilage in orthopedic bearing applications. Although these materials provide excellent shock absorption and lubricant transfer when compared to UHMWPE, their poor mechanical properties and resulting poor wear performance limit their immediate value in artificial joints. Oka *et al* and Suciu *et al* both report hydrogel wear rates at least an order of magnitude greater than rates typically seen in

non-crosslinked UHMWPE [44, 45], while interactions between the hydrated hydrogel and natural lubricants create a complex tribological process that makes long term behavior difficult to predict [46].

Although not as predominant as hydrogels in the field of tissue engineering, porous UHMWPE porous scaffolding has been investigated for non-load bearing medical applications due to its ease of manufacturing, durability, chemical inertness and biocompatibility. Frequently used in facial reconstruction surgeries [47] and filtration membranes [48], such components are often created through a porogen leaching process in which the samples are initially created with an dissolvable porogen, such as salt, dispersed throughout the sample. The sample is then soaked in a solvent that dissolves away the porogen, leaving voids within the polymer. Leaching techniques are cost effective solutions for producing a wide range of polymeric porous structures [49-52]. Even when held at a constant porosity, controlling the size and shape of the porogen also can result in variable mechanical properties [53, 54].

Typical studies into porous UHMWPE leave the pores vacant, allowing for cell in-growth or fluid flow through the sample. However, filling the pores of porous UHMWPE with a complimentary material, such as a hydrogel, may result in distinct advantages for artificial joint applications. On a basic level, the hydrogel phase could be infiltrated with bone morphogenetic protein (BMP) such that as the acetabular cup begins to wear, BMP is released into the joint, counteracting the osteolytic effect of the wear particulate. Tailoring the ratio of hydrogel to UHMWPE could create an ideal balance of wear resistance, shock absorption, and lubrication, reducing wear and

extending the functionality of the joint. With osteolysis a non-issue, it is unlikely that the cup would need replacement, so the porous nature could be tuned to allow for cell in-growth along the back of an implant, creating more permanent fixation of the implant to the surrounding bone.

This work represents an effort towards study combining the strengths of both UHMWPE and hydrogels by impregnating porous UHMWPE with a hydrogel. First, the creation of tailored porous UHMWPE through porogen leaching was examined through mathematical models and parallel physical experiments. Porous samples were then impregnated with gelatin to observe the interaction and penetration of a hydrogel in a hydrophobic scaffold.

3.2 Materials and Methods

Numerical Modeling

To create a porous UHMWPE scaffold through salt leaching, a UHMWPE composite with well-dispersed salt granules is a necessary first step. To achieve this, granulated UHMWPE was dry mixed with salt crystals, then compressed under heat and pressure into a solid block. Previous studies by the authors of UHMWPE composites created using the same process suggested that the ratio of matrix particle size to filler particle size greatly influenced the final distribution of filler particles within the fully formed composite. In an effort to understand the relationship between the porogen (salt)

and polymer particles during the dry powder mixing process, a simple numerical model was created in Matlab to represent the distribution of particles within a sample volume.

The basic strategy of this "powder dispersion" model was to create a visual representation of a two dimensional slice of a final composite based on the volume percent and initial particle size of the two constituents. An empty 2-D array represented a sample area, and Representations of individual particles filled a certain number of indices within the array depending on the material type represented. A virtual particle, either porogen or matrix type, was randomly placed along the top of the array, and then lowered through the empty space until another particle was encountered. This position in the array was then filled, and another particle began the process. This was repeated until the array was filled. This program allowed for visual comparison of the particle distribution associated with various particle sizes.

A second numerical model was created to demonstrate the behavior during the leaching process. A three dimensional array representative of a sample volume was filled with the appropriate number and size of randomly placed porogen particles. This array was then subjected to a virtual leaching process by removing porogen particles that were exposed to an outside surface or empty region. As particles were removed, new empty regions were created within the matrix. Starting out the outside edges and working inward, the rinsing process repeated until no further porogen particles could be removed. The final porosity and remaining volume percent of porogen was then calculated. This allowed for comparisons of multiple samples with varied porogen concentrations and particle sizes.

Physical Sample Creation

Sodium chloride (*OmniPur*, EMD), was chosen as a porogen due to its availability, solubility in water, and biocompatibility. To control the particle size, salt was ground with a mortar and pestle, then sieved into two separate batches: one consisting of particles less than 100 μm, and the other of particles between 100-300 μm. The two different batches will be referred to as small and large particles, respectively. Granulated UHMWPE (GUR-1050, Ticona) with an average particle size approximately 140 μm was added to the particles to create multiple powder mixtures ranging from 10 to 85 percent salt, by weight, all of which were mixed in a vortex mixer. These mixtures were then compression molded at 230° C and 100 MPa for 10 minutes to create cylindrical samples 6.54 mm in diameter and approximately 15 mm long.

After formation, the sample weights were recorded. The samples were placed in a beaker of water in an ultrasonic bath for a total of 5 hours to leach out the imbedded salt. The water was replaced every 30 minutes during the first 2 hours of soaking, then periodically throughout the rest of the soak cycle. At the completion of the leaching process, all the samples were thoroughly dried and weighed. The weight loss of each sample was compared to the predictions made by the three dimensional numerical model.

Sample Imaging

After leaching, selected samples were imaged in a JOEL-6400 scanning electron microscope. Samples were prepared for imaging first with a ruthenium vapor coating

technique [28], then with a light sputter coating of gold-palladium. The ruthenium vapor coating creates a more even coating on highly mottled surfaces than sputter coating would alone.

Dynamic Mechanical Analysis

Selected powder mixtures, along with unfilled UHMWPE powder, were chosen to create samples for dynamic mechanical analysis (DMA), which were compression molded at 230° C and 4 MPa into 63x12.5x4 mm rectangular beams. These samples were leached and dried according the procedure described above. The storage and loss modulus of each sample was measured at room temperature by a Q800 TA Dynamic Mechanical Analyzer with a three-point bending apparatus.

Impregnation

To prove the viability of using porous UHMWPE as structural scaffoldings for various soft tissues and gels, leached and dried samples were impregnated with gelatin, and then imaged in the SEM. A procedure for preparing samples was developed specifically for SEM imaging, and is described below. This chemical treatment process allows the gelatin to retain its structure while under the high vacuum of the SEM, and improves the contrast between the UHMWPE scaffolds and the gelatin when viewed with backscattered electron detection through the addition of gold nanoparticles to the gelatin phase. This procedure would not be necessary for generic preparation of mechanical samples.

0.35 grams of gelatin (Knox) was mixed with colloidal gold (25 nm diameter, Anderson Laboratories) in 10 mL distilled water. This mixture was heated to a boil, then the cylindrical porous UHMWPE samples were submerged into the resulting liquid. The entire setup was placed under intermittant vacuum of 380 mm Hg to increase the penetration of the gelatin into the pores of the UHMWPE. After 15 minutes under vacuum, the mixture was chilled in a refrigerator for 2-3 hours to gel, after which, the now impregnated UHMWPE samples were removed. These samples were immediately placed into a 10% (vol/vol) aqueous acrolein (Electron Microscopy Sciences) solution to crosslink the gelatin, preventing the structure from degrading during the drying process. After crosslinking, samples were rinsed in three changes of deionized water and then dehydrated in successive concentrations of methyl alcohol in water, ranging from 10% to 100% alcohol. Finally, thin slices from the centermost region of the samples were removed using a fresh razor blade. These sections were then submerged in three changes of hexamethyldisilazane (HMDS, Electron Microscopy Sciences) a chemical critical point drying solution, then carbon coated for viewing under the SEM.

3.3 Results and Discussion

Modeling Results

The powder dispersion model described above creates visual representation of cross-sections of a virtual sample. The scale of both axes is given as multiples of the smallest particle dimension. Representations of particle distributions for a variety of

initial particles sizes were created using the powder dispersion model. For every run, both the volume percent and porogen particle size were held constant while the initial size of the matrix particles was increased. These results, summarized in Figure 8, revealed distinct differences in the dispersion quality as the ratio of matrix to porogen particle sizes increased. The particle size ratio of 1:1 (matrix:porogen) generates a mixture that is most uniform. As the ratio increases, the dispersion quality decreases.

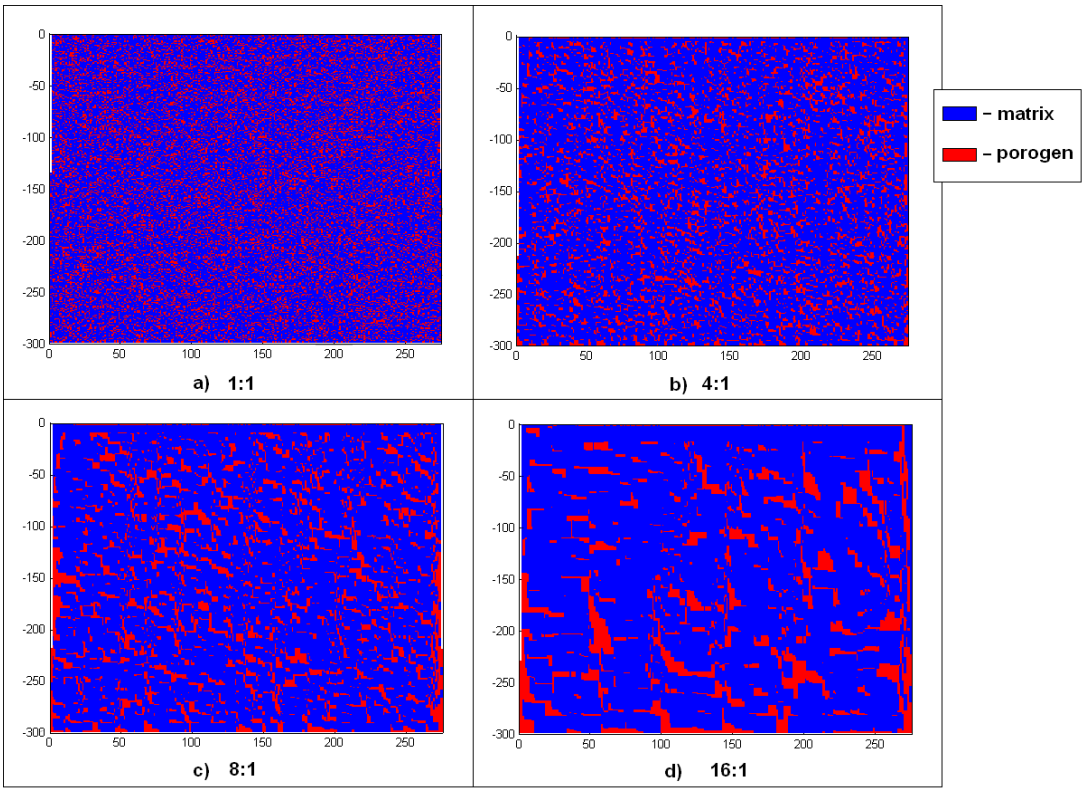

Figure 8: Representations of sample cross-sections from a numerical model which simulates the distribution of porogen and matrix particles during dry powder mixing. The porogen particle size is the same in all images, while the matrix particle size increases in successive images. The ratio of matrix particle size to porogen particle size is a) 1:1, b) 4:1, c) 8:1, and d) 16:1.

When in powder form, the position of two individual particles cannot overlap. This limits the position of the porogen particles to the regions outside of the matrix particles, regardless of the fill content of the mixture or the diameter of either particle. If the individual matrix particles are significantly larger than the porogen particles, the region in which porogen particles cannot penetrate is also large. This requires the porogen particles to accumulate together around the edges of matrix particles. Therefore, the larger the matrix particles are in relation to the porogen particles, the less uniform the resultant powder mixture will be.

In most composite applications, the ideal mixture is uniform, implying that the ideal particle size ratio is 1:1. In the cases of much higher ratios, for the final product to become uniform, the porogen particles would have to migrate away from each other through the melted matrix during the molding process. This would require that the porogen particles have no mutual attraction, and that the duration of elevated temperature allows for complete diffusion. In this study, the high melt viscosity of UHMWPE prevents this particle motion.

While typical composite applications seek uniform particle distributions, the leaching process does not necessitate such uniformity. It requires only that the salt particles achieve percolation to allow for full leaching, and that the matrix remains interconnected so that the resulting porous structure remains in one piece. In this regard, using a size ratio greater than 1:1 may prove beneficial by forcing the salt particles to accumulate in interconnected veins that run through the entirety of the sample, allowing for percolation of at lower fill contents. Using this technique would

also result in the many of the final pores to be much greater in size than the individual porogen particle size due to the accumulation of particles, even at low fill contents. To explore these phenomena, physical samples were made with two different sizes of porogen particles: one batch approximately equal to the matrix particle size, while the other batch contained particles much smaller than the matrix particles.

Leaching Model

The three dimensional leaching model predicted the total volume of porogen that could be released dependent on sample geometry, pore size, and fill content. The numerical simulation outputs the porosity of the sample after the leaching process, that is, the percentage of the original sample volume that becomes void after leaching. An example of the results is found in Figure 9.

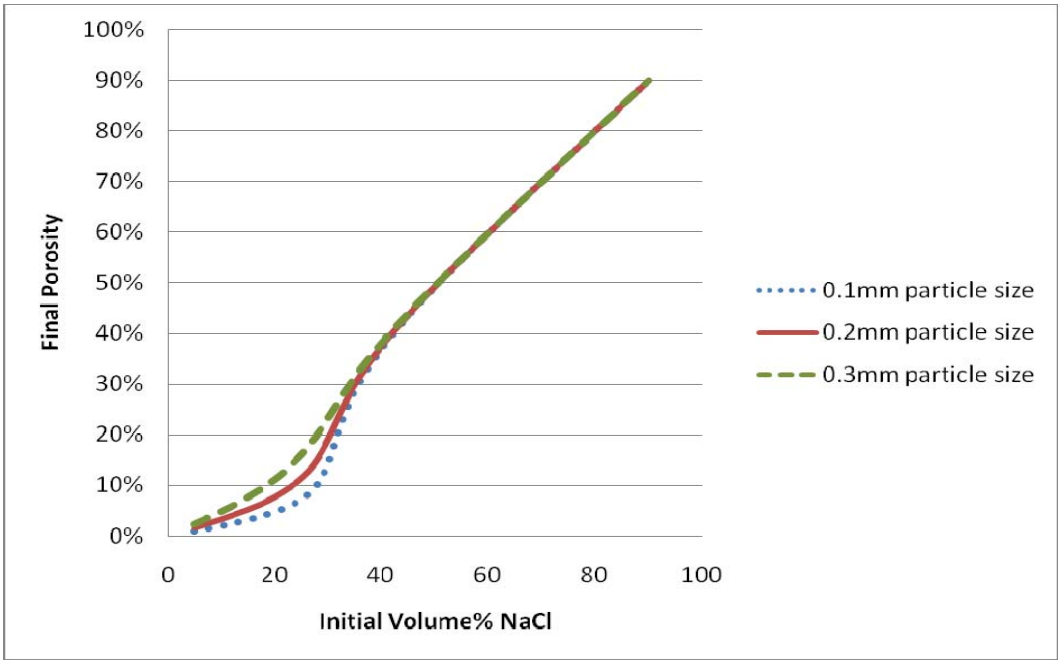

Figure 9: Numerical model predictions of final porosity for a 6x6x15mm sample filled with porogen particles of varying size.

Of particular interest is the discrepancy between samples of the same fill content but different porogen particle sizes. The numerical model predicts that smaller pore sizes will result in lower final porosity, meaning that more porogen remains within the matrix after leaching. This result can be explained by the manner in which the model handles particle placement. As previously mentioned, this model assumes a random dispersion of porogen particles, implying that each particle has a specific likelihood that it will connect with another particle. This probability is dependent on the volume percent of porogen within the sample, but not the particle size. When considering interconnected networks, the propogation of probability requires that longer chains of multiple particles are less likely than chains of fewer particles.

For the leaching process to remove all the porogen, an interconnected network of porogen particles must begin at an outer surface of the sample and extend into the center of the sample volume. The total number of particles required to span this distance increases as the size of individual particles decreases. Therefore, for a given sample size and fill content, a smaller particle size has a lower probability of generating chains sufficiently long enough to reach the centermost porogen particles, resulting in a lower final porosity after leaching. It is important to note that this result is only valid with randomly distributed porogen particles. This condition only applies to the larger pore size, as predicted by the two dimensional model.

For the samples created with smaller porogen particles, the powder dispersion model predicts the accumulation of vein-like bands of particles throughout the sample. It was expected that these structures would improve percolation, especially at lower fill contents, resulting in a final porosity that exceeds the randomly dispersed leaching model results. To prove this concept and verify both numerical models validity, a range of physicals samples were created according to the method previously described. These samples were weighed before and after leaching to compare to the model. Figure 10 summarizes this data.

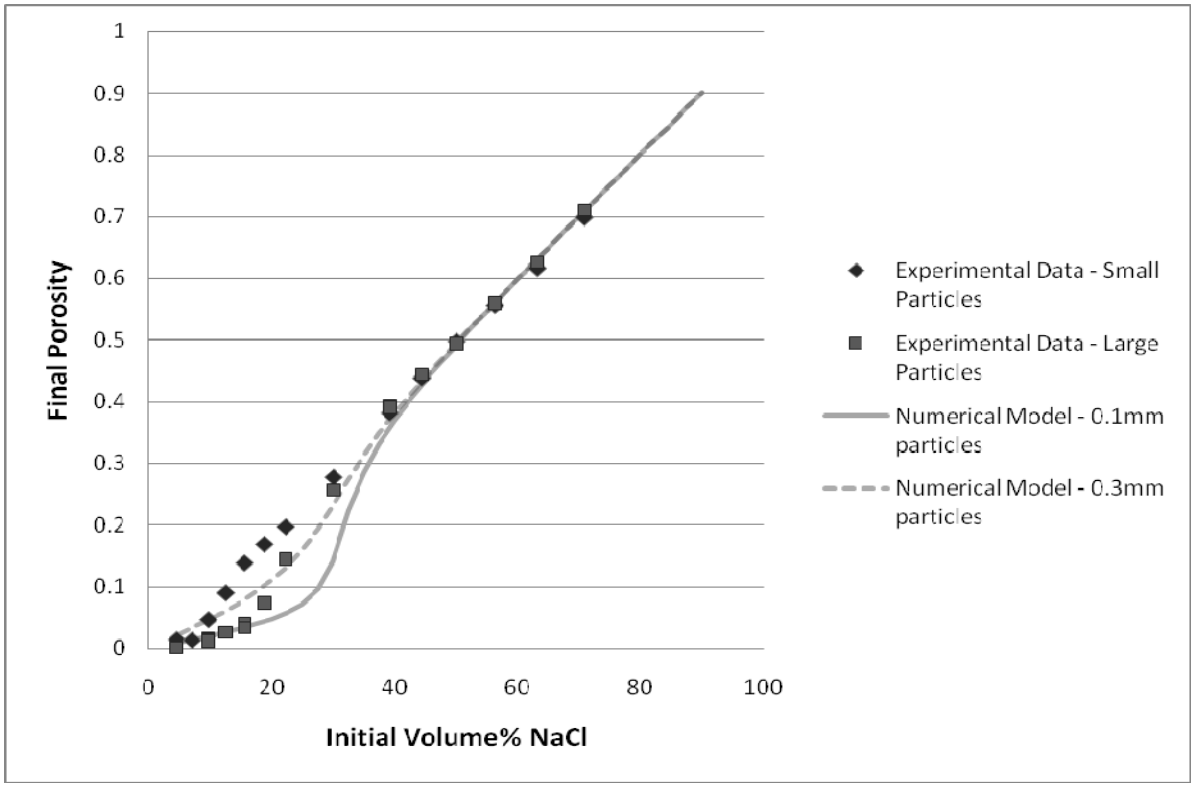

Figure 10: Final Porosity results: theoretical predictions and experimental data.

The experimental data for samples made with large particles (100-300 μm) matches well with the leaching model results for similar pore sizes, suggesting that the leaching model is valid for samples created with a particle size ratio of approximately 1:1. The data collected from samples created from smaller particles matches well with predictions at high fill contents, but exceeds the predicted porosity at lower fill contents. This result supports the theory of particle accumulation when initial particle sizes are not equal. In both cases, samples made with initial fill contents greater than 40 volume percent released 90 percent or more of their total salt during the leaching process.

To examine the internal porous structure, the physical samples were sliced in half with a razor blade, and the exposed surface was imaged in an SEM. These images can be seen in Figure 11. Samples with larger particle sizes revealed a well defined porous structure defined by single cubic salt crystals. Pores were interconnected through the overlapping of large single crystal formations, and the interior walls of the pores appeared relatively smooth. In contrast, the samples made with smaller salt particles revealed a less orderly porous structure. Within these samples, the larger regions of pores were not uniform in size or geometry, and were interconnected through thin branching of smaller pores. Interior surfaces were noticeably rougher than in samples made from large particles. This type of structure is consistent with the marbled appearance and particle accumulation predicted by the two dimensional model. These results support the claim that the average pore size, geometry, and porosity can be tailored through the control of the porogen and matrix particle size and quantity.

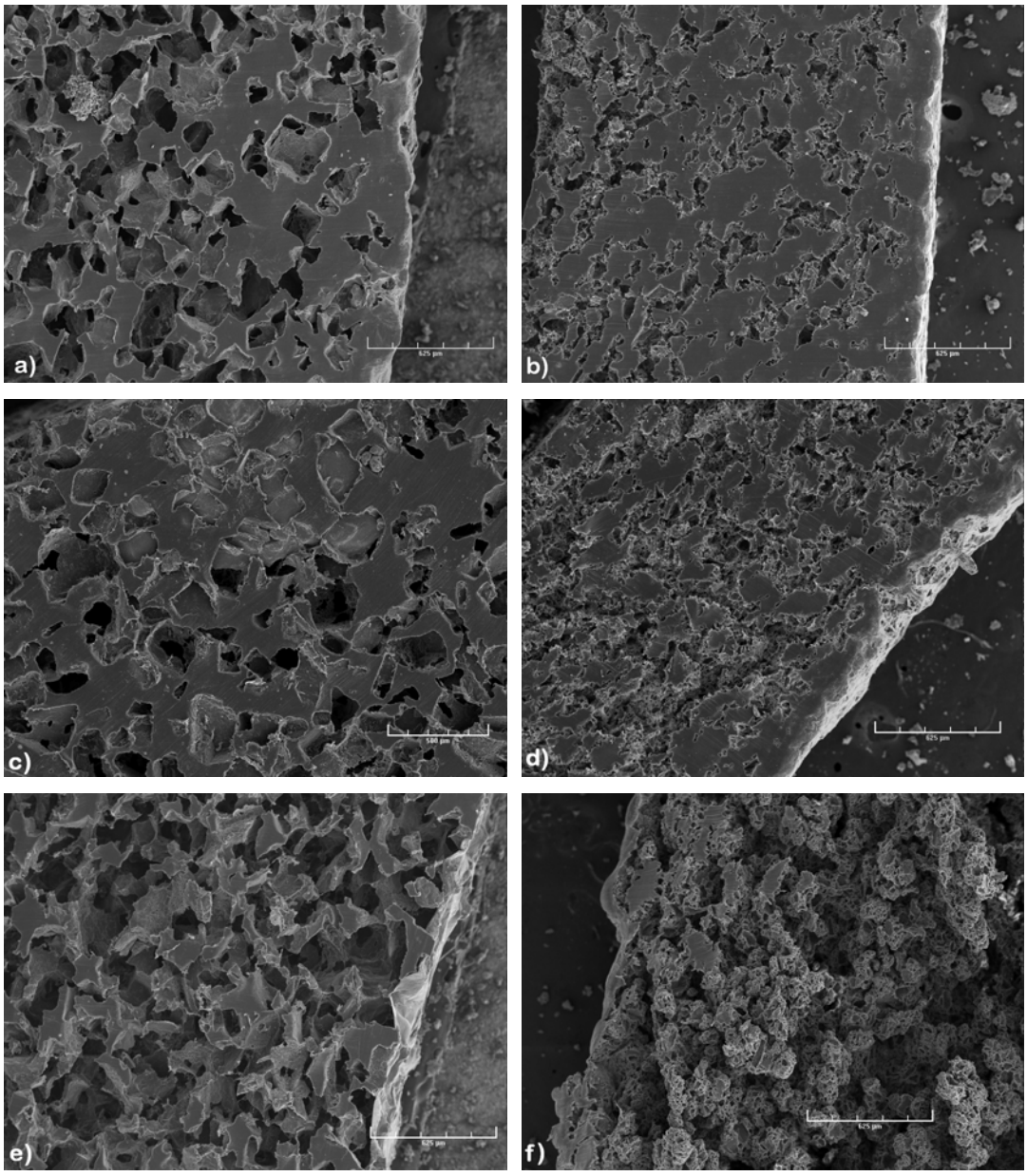

Figure 11: SEM images of porous UHMWPE structures created through salt leaching. (a) large pores, 30vol%; (b) small pores, 30vol%; (c) large pores, 50vol%; (d) small pores, 50vol%; (e) large pores, 63vol%; (f) small pores, 70vol%;

Dynamic Mechanical Analysis

The results of the dynamic mechanical analysis can be seen in Figures 12 and Figure 13. The measured storage and loss moduli for solid UHMWPE match well with literature. It was suspected that the moduli would decrease in direct relation to the percent of volume lost during leaching, meaning that a sample that was 50% porous by volume would be 50% as strong as a solid sample. However, the DMA results show that a sample that lost 22% volume during leaching had its storage modulus decreased by 55%.

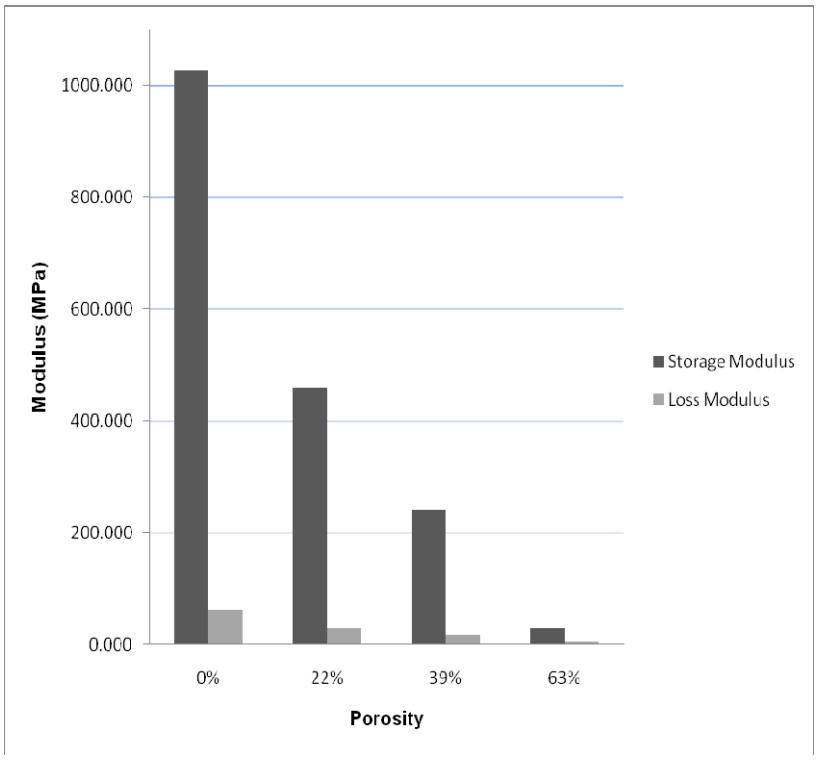

Figure 12: DMA measurements of storage and loss modulus for porous samples made with varying contents of small NaCl particles.

A comparison between a sample made with large NaCl particles and one made with small particle revealed virtually no difference in storage and loss modulus, suggesting that at this particular fill content, the initial particle size has little effect on modulus. More samples covering a wider range of porosities would be required to make a more general statement about particle size influence. This is especially true for samples with low fill contents, when small particles achieve percolation, but large particles do not. Also to be considered, pores created with the small particles can be significantly larger than the size of an individual particle due to particle accumulation.

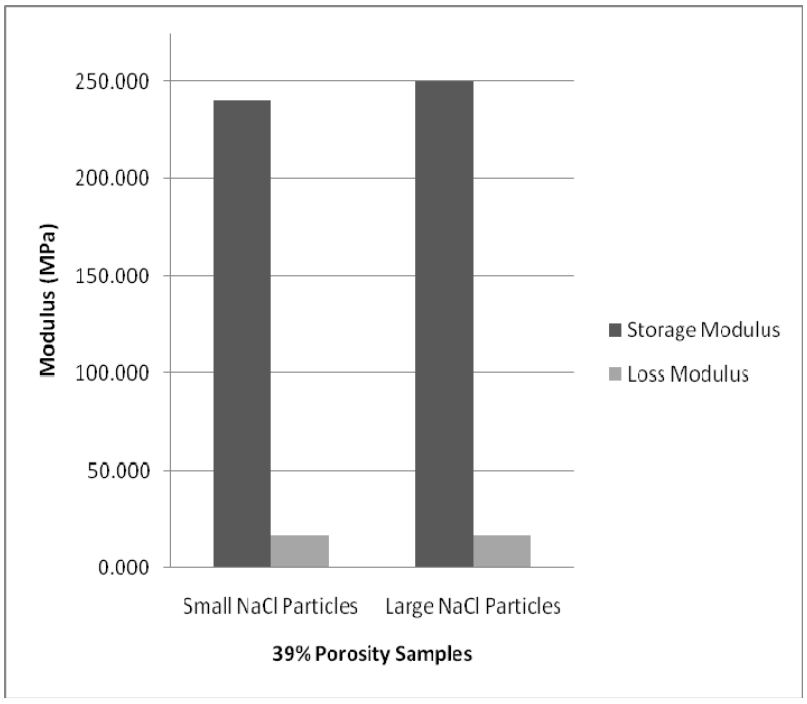

Figure 13: Comparison of storage and loss modulus for samples made from large and small NaCl particles.

Impregnation with Gelatin

Samples were impregnated with gelatin according to the procedure described above, then SEM images were taken using both secondary and backscatter mode to reveal the structure of the composite. The secondary images revealed the overall distribution and geometry of pores, but offered very little information regarding behavior of the gelatin. As seen in Figure 14, the backscattered images clearly showed the location of gelatin within the polymer scaffolding while hiding the complex surface topography.

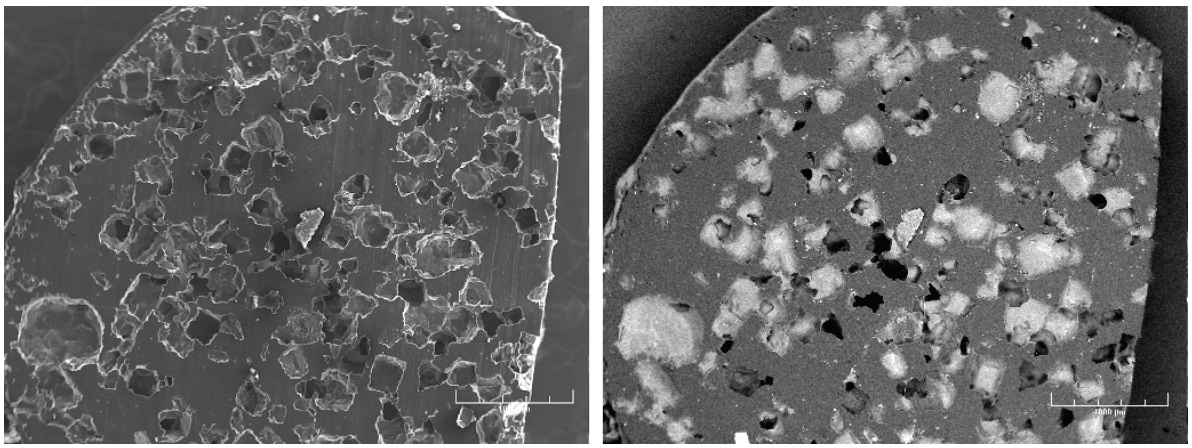

Figure 14: Secondary image (left) and backscattered image (right) of a 30% porous sample made from large NaCl particles. Pores successfully impregnated with gelatin glow brightly in backscattered images.

A variety of impregnated samples can be seen in Figure 15. In all samples, the gelatin was able to penetrate completely to the centermost regions of the circular cross

section. Samples made from smaller particles had regions of small branched pores resulting gelatin branches which were thinly spread and not as bright in backscatter mode, making image analysis challenging. The samples made with large pores in the UHMWPE appeared to have a greater extent of volume filled with the gelatin phase.

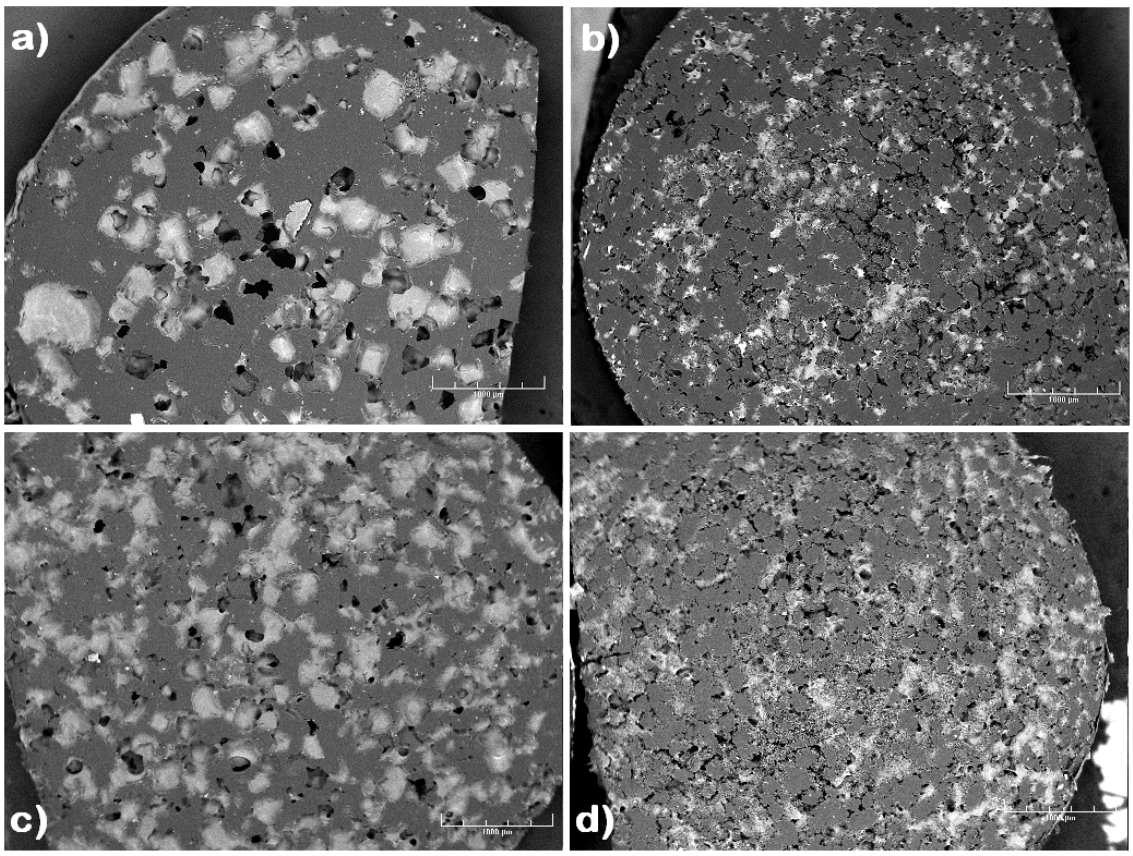

Figure 15: Comparison of gelatin penetration for samples made with (a) 30% porous, large particles; (b) 30% porous, small particles; (c) 50% porous, large particles; (d) 50% porous, small particles.

Every sample also contained a fraction of unfilled voids. Figure 16 shows magnified images of voids found in samples created with large pores. These images identify two possible situations for void formation: 1) entrapped air pockets and 2) channels which are too small for viscous gelatin to flow through. The first situation, entrapped air pockets, is represented by the locations marked “a” in Figure 9, and is characterized by a void that is surrounded by gelatin for part of it boundary. This interface creates a markedly smooth and rounded surface on the gelatin, making their occurrence easy to identify. Better saturation of the porous scaffold could be achieved by degassing the gelatin before impregnation, keeping the gelatin warm to decrease viscosity during the impregnation process, or applying the vacuum for longer during the curing process. Mechanical agitation during the impregnation process might also be beneficial by coercing air bubbles to find paths to the external surface of the scaffold. Entrapped air pockets account for the majority of voids visible in all samples.

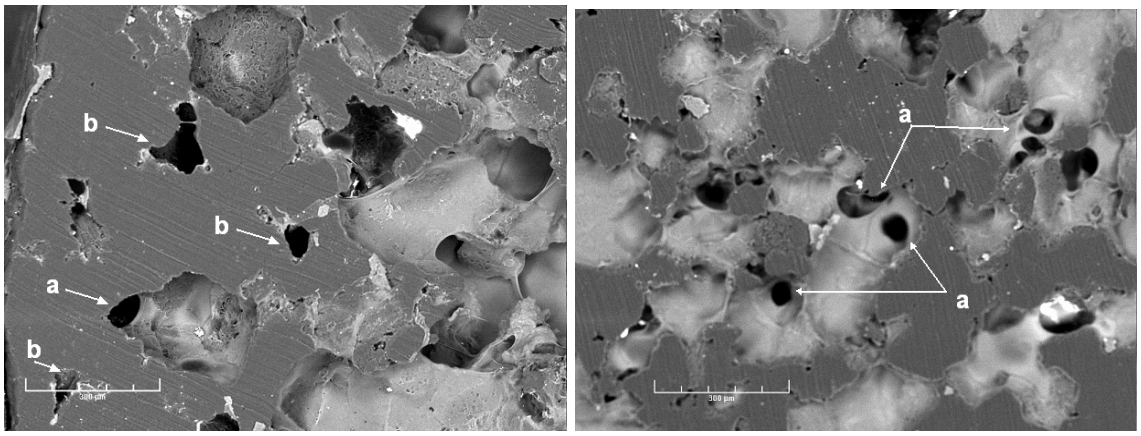

Figure 16: Backscattered images of voids in a porous sample made using large NaCl particles. The void at location (a) represents a pocket of air entrapped by gelatin, while the void at (b) shows no presence of gelatin within the pore.

The voids at locations identified as "b" appear to be completely isolated from all other pores, or only connected to another pore through a very small channel. These types are much more difficult to identify due to the limited view of the SEM into the three-dimensional porous structure. It is possible that these voids are simply extensions of trapped air pockets, and the identifiable interfaces are either hidden beneath the surface or were removed during sample preparation. A second possibility is that neighboring pores were only interconnected by small channels through which water could flow during the leaching process, but the more viscous gelatin was unable to flow through. Figure 17 demonstrates the limitations of gelatin flow through small channels. The channel at location "c" measures approximately 20 μm in width, and is clearly large enough for gelatin to flow through. The neighboring channel at "d" measures approximately 10 μm in width, small enough to prevent gelatin flow. The same basic

strategies suggested to aid against air pockets entrapment will benefit in these small channel situations as well.

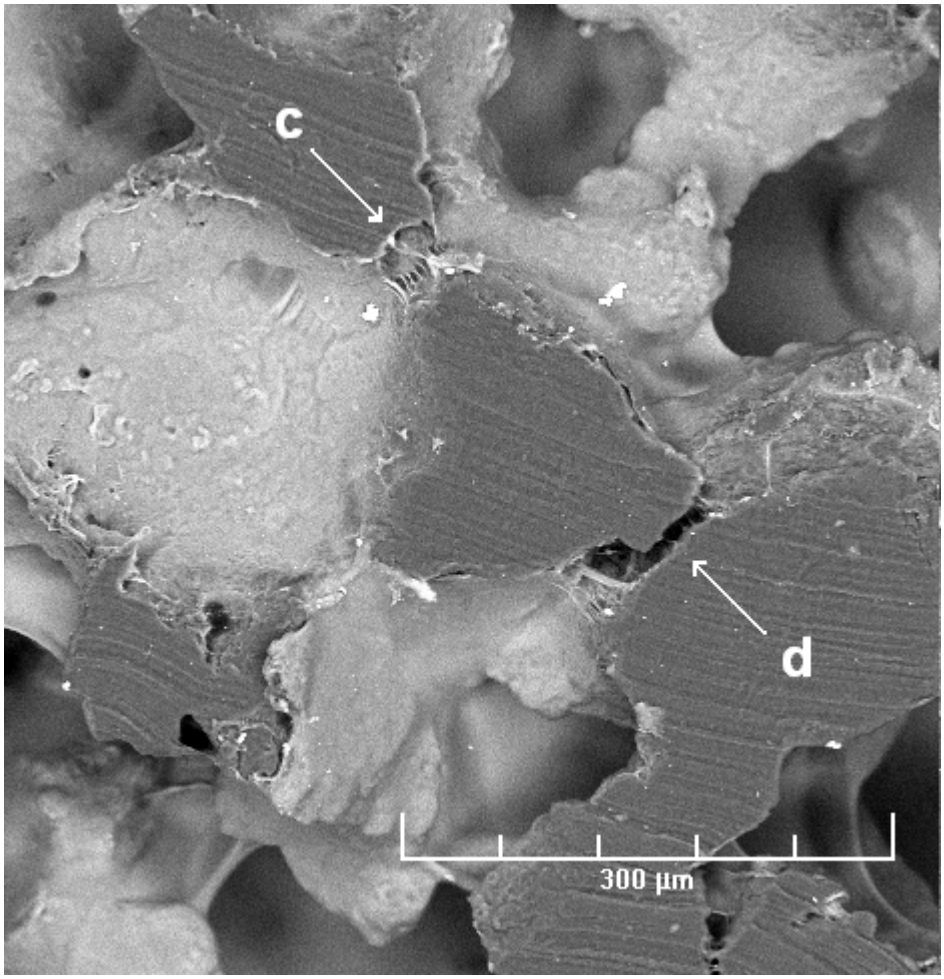

Figure 17: Gelatin can flow through the narrow channel at (c), which measures 20 µm across. However, gelatin does not flow through channel (d), which measures only 10 µm across.

There is a third case which has not yet been addressed. If a salt particle is completely isolated within the matrix, it will not be washed away during the leaching process. However, when the sample is sliced open in preparation for imaging, the isolated particle could be pulled free from the matrix, leaving an isolated and empty pore behind. A similar result would occur if the portions of gelatin were pulled out of the pores during sample cutting.

Regardless of the quantity and cause of voids within the composite, it is apparent that for every case in this study, the gelatin phase was able to permeate throughout the majority of the UHMWPE scaffold, and the gelatin conformed to the size and geometry of the pores within the scaffold. This opens the door for future research using porous UHMWPE as scaffolding for other hydrogels and bio-derived polymers.

3.4 Conclusions

1. When using a dry powder mixing technique, uniform distributions can be achieved when all particles are of a similar size. If one constituent is larger than the other, the smaller particles collect in vein-like bands that run throughout the sample. The greater the size difference between particles, the less homogenous final distribution will be.

2. The inhomogeneous, vein-like accumulations seen in samples of mismatched particle sizes allows for percolation to be achieved at lower fill contents.

3. Numerical simulations can be used to predict the resulting porous structure for porogen leaching processes with reasonable accuracy.

4. A porous sample will have a significantly lower modulus than a solid sample. The percentage of decrease in modulus will be greater than the percentage of volume that is open pore.

5. Porous UHMWPE created through salt leaching is an inexpensive and effective method for creating tailored scaffolding structures for supporting hydrogels and other bio-derived materials.

4. GENERAL CONCLUSIONS

Artificial joints are becoming more commonplace in today's society, especially within younger patients, thus necessitating the development of components with longer life expectancies. Ultra-high molecular weight polyethylene has long been the material of choice in these applications, and the results presented in study suggest that the use of UHMWPE will continue for years to come, only now in the form of composites.

Filling UHMWPE with zirconium successfully reduces wear while maintaining impact toughness. Although more research is needed to determine *in vivo* performance of such composites, the path to actual product implementation would be relatively quick and easy, especially since zirconium is already used in orthopedic applications.

Meanwhile, research should focus on developing new bio-friendly composites using porous UHMWPE as scaffoldings. This branch of research is still in its infancy, so the path to implementation of such composites would take much longer than the zirconium filled composite; however, the rewards are much greater. As opposed to simply slowing the osteolytic effect, these composites have the potential to completely eliminate osteolysis, while at the same time creating more natural conditions within the joint and surrounding tissue. Porous UHMWPE scaffolds can be precision tuned to a variety of properties, then filled with any number of beneficial materials, making this technology reach far beyond just artificial joints, potentially benefitting the lives of millions.

.

REFERENCES

[1] S. Dawlee, A. Sugandhi, B. Balakrishnan, D. Labarre, A. Jayakrishnan, Oxidized chondroitin sulfate-cross-linked gelatin matrixes: A new class of hydrogels, Biomacromolecules 6 (2005) 2040-2048.

[2] J. B. Leach, K. A. Bivens, C. W. Patrick, C. E. Schmidt, Photocrosslinked hyaluronic acid hydrogels: Natural, biodegradable tissue engineering scaffolds, Biotechnology and Bioengineering 82 (2003) 578-589.

[3] Q. Li, C. Williams, D. Sun, J. Wang, K. Leong, J Elisseeff, Photocrosslinkable polysaccharides based on chondroitin sulfate, Journal of Biomedical Materials Research 68A (2003) 28-33.

[4] J. H. Dumbleton, M. T. Manley, A. A. Edidin, A literature review of the association between wear rate and osteolysis in total hip arthroplasty, Journal of Arthroplasty 17 (2002) 649-661.

[5] N. D. L. Burger, P. L. de Vaal, J. P. Meyer, Failure analysis on retrieved ultra high molecular weight polyethylene (UHMWPE) acetabular cups, Engineering Failure Analysis 14 (2007) 1329-1345.

[6] R. Chiesa, M. Moscatelli, V. Gonzalez-Mora, M. Hoffman, Mechanical properties and wear performance of crosslinked UHMWPE for orthopedic joints, Proceedings of IEEE-EMBS Special Topic Conference on Molecular, Cellular and Tissue Engineering (2002) 58-59.

[7] G. Lewis, Properties of crosslinked ultra high molecular weight polyethylene, Biomaterials 22 (2001) 371-401.

[8] H. A. Khonakdar, J. Morshedian, U. Wagenknect, S. H. Jafari, An investigation of chemical crosslinking effect on properties of high-density polyethylene, Polymer 44 (2003) 4301-4309.

[9] E. Oral, S. D. Christensen, A. S. Malhi, K. K. Wannomae, O. K. Muratoglu, Wear resistance and mechanical properties of highly cross-linked, ultrahigh-molecular weight polyethylene doped with vitamin E, Journal of Arthroplasty 21 (2006) 580-591.

[10] L. A. Pruitt, Deformation, yielding, fracture and fatigue behavior of conventional and highly cross-linked ultra high molecular weight polyethylene, Biomaterials 26 (2005) 905.

[11] P. Taddei, S. Affatato, C. Fagnano, A. Toni, Oxidation in ultrahigh molecular weight polyethylene and cross-linked polyethylene acetabular cups tested against roughened femoral heads in a hip joint simulator, Biomacromolecules 7 (2006) 1912-1920.

[12] Y. S. Liao, H. McKellop, Z. Lu, P. Campbell, P. Benya, The effect of frictional heating and forced cooling on the serum lubricant and wear of UHMW polyethylene cups against cobalt-chromium and zirconia balls, Biomaterials 24 (2003) 3047-3059.

[13] C. Piconi, G. Maccauro, Zirconia as a ceramic biomaterial, Biomaterials 20 (1999) 1-25.

[14] M. Zhang, P. Pare, R. King, A novel ultra high molecular weight polyethylene-hyaluronan microcomposite for use in total joint replacements. Mechanical and tribological property evaluation, Journal of Biomedical Materials Research 82A (2007) 18-26.

[15] L. Fang, Y. Leng, P. Gao, Processing and mechanical properties of HA/ UHMWPE nanocomposites, Biomaterials 27 (2006) 3701-3707.

[16] M. T. Khorasani, M. Zaghiyan, H. Mirzadeh, Ultra high molecular weight polyethylene and polydimethylsiloxane blend as acetabular cup material, Colloids and Surfaces B: Biointerfaces 41 (2005) 169-174.

[17] H. Mahfuz, A. Adnan, Manufacturing and characterization of carbon nanotube /polyethylene composites, National Journal of Nanoscience 4 (1) (2005) 55-72.

[18] S. Ruan, S. Ruan, P. Gao, T. X. Yu, Ultra-strong gel-spun uhmwpe fibers reinforced using multiwalled carbon nanotubes, Polymer 47 (2006) 1604.

[19] Y. Xue, W. Wu, O. Jacobs, B. Schadel, Tribological behaviour of UHMWPE /HDPE blends reinforced with multi-wall carbon nanotubes, Polymer Testing 25 (2006) 221-229.

[20] C. Deshmane, Q. Yuan, R. S. Perkins, R. D. K. Misra, On striking variation in impact toughness of polyethylene-clay and polypropylene-clay nanocomposite systems: The effect of clay-polymer interaction, Materials Science and Engineering: A 458 (2007) 150-157.

[21] D. S. Xiong, J. M. Lin, D. L. Fan, Wear properties of nano-Al_2O_3/UHMWPE composites irradiated by gamma ray against a CoCrMo alloy, Biomedical Materials 1 (2006) 175-179.

[22] M. Tanniru, R. D. K. Misra, On enhanced impact strength of calcium carbonate-reinforced high-density polyethylene composites, Materials Science and Engineering: A 405 (2005) 178-193.

[23] C. J. Schwartz, S. Bahadur, S. K. Mallapragada, Effect of crosslinking and Pt-Zr quasicrystal fillers on the mechanical properties and wear resistance of UHMWPE for use in artificial joints, Wear 263 (2007) 1072-1080.

[24] C. Z. Liu, C. Z. Liu, L. Q. Ren, J. Tong, S. M. Green, R. D. Arnell, Effects of operating parameters on the lubricated wear behavior of a PA-6/ UHMWPE blend: A statistical analysis, Wear 253 (2002) 878.

[25] H.W. Fang, Y.-C. Su, C.-H. Huang, C.B. Yang, Influence of biological lubricant on the morphology of UHMWPE wear particles generated with microfabricated surface textures, Materials Chemistry and Physics 95 (2006) 280-288.

[26] C. Schwartz, S. Bahadur, Development and testing of a novel joint wear simulator, and investigation of the viability of an elastomeric polyurethane for total joint arthoplasty devices., Wear 262 (2007) 331-339.

[27] ASTM F 648-04, Determination of the Impact Resistance of Ultra High Molecular Weight Polyethylene, Annual Book of ASTM Standards, ASTM International, 2007.

[28] G. M. Brown, J. H. Butler, New method for the characterization of domain morphology of polymer blends using ruthenium tetroxide staining and low voltage scanning electron microscopy (LVSEM), Polymer 38 (1997) 3937-3945.

[29] R. Chiesa, M. C. Tanzi, Alfonsi, Paracchini, Moscatelli, Cigada, Enhanced wear performance of highly crosslinked UHMWPE for artificial joints, Journal of Biomedical Res. 50 (2000) 381-387.

[30] O. Muratoglu, D. O'Connor, C. Bragdon, J. Delaney, M. Jasty, *et al*, Gradient crosslinking of UHMWPE using irradiation in molten state for total joint arthroplasty, Biomaterials 23 (2002) 717-724.

[31] M. Jasty, H. E. Rubash, O. Muratoglu, Highly cross-linked polyethylene: The debate is over--in the affirmative, Journal of Arthroplasty 20 (2005) 55-58.

[32] M. D. Ries, Highly cross-linked polyethylene: The debate is over--in opposition, Journal of Arthroplasty 20 (2005) 59-62.

[33] R. Chiesa, M. Moscatelli, V. Gonzalez-Mora, M. Hoffman, Mechanical properties and wear performance of crosslinked UHMWPE for orthopedic joints, Molecular, Cellular, and Tissue Engineering (2002) 58-59.

[34] G. Guofang, G. Guofang, Y. Huayong, F. Xin, Tribological properties of kaolin filled UHMWPE composites in unlubricated sliding, Wear 256 (2004) 88.

[35] X. Xie, C. Tang, K. Chan, X. Wu, C. Tsui, C. Cheung, Wear performance of ultrahigh molecular weight polyethylene/quartz composites, Biomaterials 24 (2003) 1889-1896.

[36] X. Dangsheng, Friction and wear properties of UHMWPE composites reinforced with carbon fiber, Materials Letters 59 (2005) 175.

[37] G. Liu, M. Xiang, H. Li, A study on sliding wear of ultra high molecular weight polyethylene/polypropylene blends, Polymer Engineering and Science, 44 (1) (2004) 197-208.

[38] L. Fang, L. Fang, P. Gao, Y. Leng, High strength and bioactive hydroxyapatite nano-particles reinforced ultrahigh molecular weight polyethylene, Composites: Part B, Engineering 38 (2007) 345.

[39] J. B. Matthews, A. A. Besong, T. R. Green, M. H. Stone, M. Wroblewski, J. Fisher, E. Ingham, Evaluation of the response of primary human peripheral blood mononuclear phagocytes to challenge with in vitro generated clinically relevant UHMWPE particles of known size and dose, Journal of Biomedical Materials Research 52 (2000) 296-307.

[40] T. R. Green, J. Fisher, J. B. Matthews, M. H. Stone, E. Ingham, Effect of size and dose on bone resorption activity of macrophages by in vitro clinically relevant ultra high molecular weight polyethylene particles, Journal of Biomedical Materials Research 53 (2000) 490-497.

[41] J. L. Tipper, A. L. Galvin, S. Williams, Isolation and characterization of UHMWPE wear particles down to ten nanometers in size from in vitro hip and knee joint simulators, Journal of Biomedical Materials Research 78A (2006) 473-480.

[42] Y. H. Zhu, K.Y. Chiu, W.M. Tang, Review: Polyethylene wear and osteolysis in total hip arthoplasty, J of Orthop Surg (Hong Kong) (2001) 91-99.

[43] J. L. Drury, D. J. Mooney, Hydrogels for tissue engineering: Scaffold design variables and applications, Biomaterials 24 (2003) 4337-4351.

[44] M. Oka, K. Ushio, P. Kumar, K. Ikeuchi, S. Hyon, T. Nakamura, H. Fujita, Development of artificial articular cartilage, Proceedings of the Institution of Mechanical Engineers, Part H: Journal of Engineering in Medicine 214 (2000) 59-68.

[45] A. N. Suciu, T. Iwatsubo, M. Matsuda, T. Nishino, A study upon durability of the artificial knee joint with PVA hydrogel cartilage, JSME International Journal Series C 47 (2004) 199-208.

[46] M. E. Freeman, M. J. Furey, B. J. Love, J. M. Hampton, Friction, wear, and lubrication of hydrogels as synthetic articular cartilage, Wear 241 (2000) 129-135

[47] T. Wellisz, Clinical experience with the Medpor porous polyethylene implant, Aesthetic Plastic Surgery 17 (1993) 339-344.

[48] G. K. Elyashevich, A. S. Olifirenko, A. V. Pimenov, Micro- and nanofiltration membranes on the base of porous polyethylene films, Desalination 184 (2005) 273-279.

[49] Q. Hou, D. W. Grijpma, J. Feijen, Porous polymeric structures for tissue engineering prepared by a coagulation, compression moulding and salt leaching technique, Biomaterials 24 (2003) 1937.

[50] K. Katoh, T. Tanabe, K. Yamauchi, Novel approach to fabricate keratin sponge scaffolds with controlled pore size and porosity, Biomaterials 25 (2004) 4255-4262

[51] C.-J. Liao, C.F. Chen, J.H. Chen, Fabrication of porous biodegradable polymer scaffolds using a solvent merging/particulate leaching method, Journal of Biomedical Materials Research 59 (2002) 676-681.

[52] F. Shutov, V. T. Ananthanarayan, Cellular UHMW polyethylene produced by non-foaming leaching technique: Morphology and properties, Journal of Cellular Plastics 38 (2002) 163-176.

[53] L. Draghi, S. Resta, M. G. Pirozzolo, M. C. Tanzi, Microspheres leaching for scaffold porosity control, Journal of Materials Science-Materials in Medicine 16 (2005) 1093-1097.

[54] J. Reignier, M. A. Huneault, Preparation of interconnected poly([epsilon]-caprolactone) porous scaffolds by a combination of polymer and salt particulate leaching, Polymer 47 (2006) 4703-4717.

VITA

Name:	Kevin Plumlee
Address:	3123 TAMU College Station, TX 77840
Email Address:	kevplumlee@gmail.com
Education:	B.S., Mechanical Engineering, Oklahoma Christian University, 2005 M.S, Mechanical Engineering, Texas A&M University, 2008